Harvesting vibration energy using nonlinear oscillations of an electromagnetic inductor

Christopher Lee, David Stamp, Nitin R. Kapania, and Jose Oscar Mur-Miranda

Franklin W. Olin College of Engineering, Needham, MA, USA 02492

ABSTRACT

Harvesting energy from ambient vibration is a promising method for providing a continuous source of power for wireless sensor nodes. However, traditional energy harvesters are often derived from resonant linear oscillators which are capable of providing sufficient output power only if the dominant frequency of input vibrations closely matches the device resonant frequency. The limited scope of such devices has sparked an interest in the use of nonlinear oscillators as mechanisms for broadband energy harvesting. In this study, we investigate the harvesting performance of an electromagnetic harvester sustaining oscillations through the phenomena of magnetic levitation. The nonlinear behavior of the device is effectively modeled by Duffing's equation, and direct numerical integration confirms the broadband frequency response of the nonlinear harvester. The nonlinear harvester's power generation capabilities are directly compared to a linear electromagnetic harvester with similar dynamic parameters. Experimental testing shows that the presence of both high and low amplitude solutions for the nonlinear energy harvester results in a tendency for the oscillator to remain in a low energy state for non-harmonic vibration inputs, unless continuous energy impulses are provided. We conclude by considering future applications and improvements for such nonlinear devices.

Keywords: nonlinear oscillation, electromagnetic energy harvesting, Duffing's Equation, vibration energy harvesting

1. INTRODUCTION

The reduction in size and power consumption of CMOS circuitry has enabled the potential for wireless sensing networks (WSNs) to provide useful real-time information for a number of distributed systems.[1] Structural health monitoring, environmental monitoring, and biomedical sensing are just a few examples of the promising applications offered by the development of miniaturized, low-power sensing networks.[2] As these networks can consist of thousands of individual sensors, the use of WSNs will be limited if each sensor must be powered by batteries that require frequent replacement, especially in hazardous or remote locations.

A possible solution is to design harvesting systems that continuously extract and store useful energy from the ambient environment. In particular, the scavenging of low frequency mechanical vibration energy from ambient environments has been the subject of an extensive body of research. Devices that harvest low frequency ($<$ 80 Hz) vibration energy typically utilize an oscillating piezoelectric, capacitive, or electromagnetic transduction mechanism to convert mechanical energy into storable electrical energy.[1] These devices are designed so that the resonant frequency of the oscillator matches the expected frequency of the input ambient vibration. For *linear* harvesting systems, in which the device oscillations can be predicted through linear equations of motion, this "frequency matching" maximizes the mechanical response of the harvester, thereby maximizing converted power.

However, one major drawback to the linear energy harvesting approach is that it assumes most of the ambient vibration energy is concentrated at a dominant frequency. In reality, almost all ambient environments have frequency spectra with a broadband distribution of vibration energy. For example, Fig. 1 shows acceleration spectral densities of a drill press and the floor of a machine shop at Olin College (frequency ranges and amplitudes of ambient vibration are also presented in Refs. 1 and 3). Note that even spectra for machinery, typically assumed to operate at a single dominant frequency, will have energy content distributed over a range of frequencies. Versatile energy harvesters must therefore be designed to harvest significant energy over a broadband spectrum of

Energy Harvesting and Storage: Materials, Devices, and Applications, edited by Nibir K. Dhar, Priyalal S. Wijewarnasuriya, Achyut Kumar Dutta, Proc. of SPIE Vol. 7683, 76830Y · © 2010 SPIE
CCC code: 0277-786X/10/$18 · doi: 10.1117/12.849895

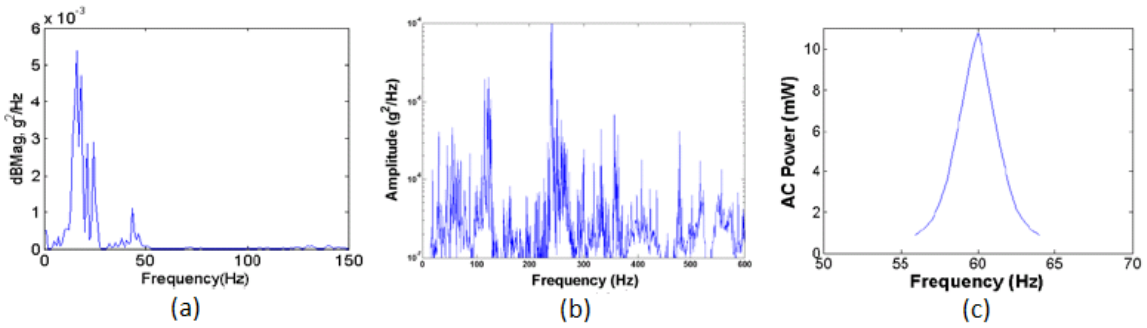

Figure 1. (a) Measured acceleration spectral densities of a drill press and the floor of a machine shop (b, amplitude factor 1e-3). (c) Frequency response amplitude for a VEH-360 Electromagnetic Vibration Harvester (Ferro Solutions Inc.)-reproduced from its specification sheet.[4] The VEH-360 displays a very narrow harvesting bandwidth, scavenging 10 mW of power at a frequency of 60 Hz but only around 2 mW of power at a frequency of 56 Hz.

frequencies. However, most commercially available energy harvesters display a very narrow harvesting bandwidth, as shown in Fig. 1.

In order to improve the performance of vibration energy harvesters, several solutions have been proposed in the literature. One investigated approach is to use a passive or active tuning mechanism to alter the natural frequency of the linear energy harvester, enabling the device to adapt to changing frequencies of ambient vibration.[5] Another approach is to increase the degrees of freedom on the linear harvester, increasing the number of resonant modes of the system, and therefore the overall system bandwidth. A multi-mass, multi-degree-of-freedom piezoelectric cantilevered beam was presented by Roundy et. al (see Ref. 5), while an L-beam piezoelectric structure with two degrees of freedom was presented by Erturk and Inman (see Refs. 6 and 7). However, it should be noted that the methods of tuning the resonant frequency and adding more degrees of freedom still leave the resulting harvester oscillations in a mostly linear domain. Designers of linear devices typically find themselves in a situation where they must decrease the damping of their harvester to achieve maximum peak power, while simultaneously increasing device bandwidth. For a linear, second-order oscillator, these goals are contradictory.

Another interesting method of increasing harvester bandwidth is to switch from devices that exhibit purely linear oscillations to those that display significant nonlinearities. Unlike a linear second-order harvester, nonlinear oscillators can have multiple stability regions and basins of attraction. Several authors have presented device designs that use nonlinear oscillations to increase harvester bandwidth. Erturk and Inman have demonstrated a piezomagnetoelastic structure that consists of a ferromagnetic cantilevered beam with two permanent magnets located symmetrically near the free end. When subjected to harmonic base excitation, the device was shown to result in a three-fold overall increase in open-circuit voltage amplitude, theoretically corresponding to a nine-fold increase in harvested power over the entire frequency spectrum.[8] A nonlinear electromagnetic harvester design has also been proposed by Mann and Sims. Using a permanent magnet sandwiched between two other permanent magnets, a device using the effect of magnetic levitation was shown to exhibit a nonlinear force/displacement relationship best modeled by a high order polynomial. Mann and Sims were able to analytically approximate and experimentally confirm the broadband frequency response of the levitation harvester.[9] This three magnet levitation device was initially studied by Defrancesco and Zanetti[10] and has also been studied by Domme.[11]

However, while both Erturk and Inman and Mann and Sims display frequency response characteristics of their proposed harvester, neither study confirmed the practicality of their devices by subjecting their harvester designs to broadband, random excitation. Both devices were tested using only a harmonic frequency sweep. Given the nonlinearity of the proposed designs, it cannot be assumed that the response to random excitation is a linear superposition of harmonic base excitations. As such devices have multiple regions of attraction, the potential for multiple stable solutions exists, making the response to random excitation difficult to predict.

Further author information: (Send correspondence to C.L.)
C.L.: E-mail: christopher.lee@olin.edu, Telephone: 781-292-2539

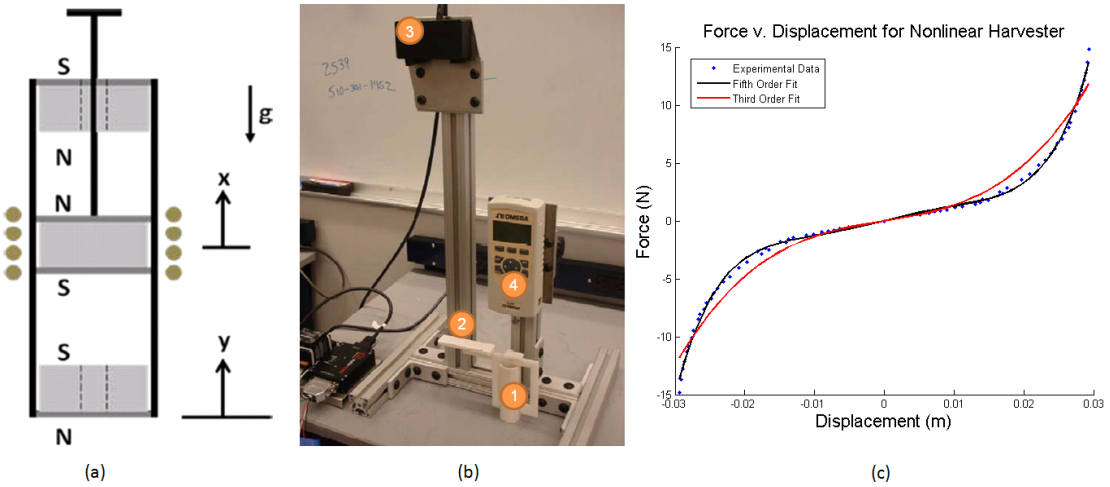

Figure 2. (a) Schematic of the nonlinear harvester. (b) Test apparatus to measure the force displacement relationship for the center magnet (1). The force acting on the center magnet and its displacement (measured via reference meter at (2) and laser displacement sensor (3)) was measured as a digital force gage (4) was lowered along a vertical track. A rectangular frame is attached to the center magnet through two axial slots in the body of the tube. (c) The force-displacement data (dots) are fitted with a cubic polynomial and a fifth order polynomial. Data was taken in one direction at a time. The static displacement (x_e = -4.2 mm) was incorporated.

To understand the practical applications of such nonlinear devices, we present a more in-depth evaluation of the three-magnet levitation harvester. First, the nonlinear relationship of such a device is characterized by examination of the force/displacement relationship. Nonlinear equations of motion are presented as a variant of Duffing's equation, and the resulting frequency responses of displacement, open source voltage, and power generation are modeled for both the nonlinear device and a frequency-matched linear device. Both devices are also fabricated, and model results for both the nonlinear and linear devices are compared to results found experimentally. Finally, both devices are subjected to uniform random vibration, where the nonlinear device is shown to exhibit difficulties in generating significant power if the input vibration is non-harmonic. We conclude by considering the changes necessary for the nonlinear harvester design to become more feasible as a broadband energy harvester.

2. EXPERIMENTAL HARVESTING DEVICES

2.1 Creating Nonlinear Oscillations with Magnetic Levitation

A schematic of the three magnet harvester configuration is shown in Fig. 2(a). The device consists of a circular permanent magnet housed in a cylindrical piece of tubing. Two permanent magnets are rigidly fixed to either end of the tube and are oriented such that the middle, unfixed magnet levitates in an equilibrium position. This permanent magnet is free to move vertically within the tube. When subjected to a base excitation $y(t)$, the center magnet oscillates with a displacement $x(t)$. A coil of wire is wrapped around the outside of the tube at the equilibrium position of the magnet, such that voltage is induced in the coil by the motion of the center magnet.

2.2 Characterization of Nonlinear Force-Displacement Relationship

Because the elastic force acting on the free magnet is created through magnetic repulsion, the relationship between the displacement $x(t)$ and the resulting elastic restoring force is nonlinear. To determine the relationship between applied force and resulting displacement, the fixture shown in Fig. 2b was used. A digital force gage was lowered, displacing the central magnet below the equilibrium position. The corresponding displacement of the central magnet was then measured with a laser displacement probe. The top and bottom magnets were then

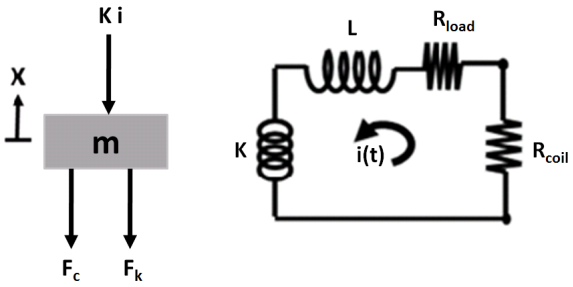

Figure 3. Free body diagram for the center magnet (left). Circuit diagram for the harvester (right). Absolute displacement from the static equilibrium position is x. Displacement of the base is y. The electro-mechanical coupling force is Ki. The motion of the magnet through the coil induces a voltage proportional to relative velocity.

interchanged and the test was repeated. The static displacement of the center magnet under gravity was also directly measured and incorporated into the force-displacement plot.

Figure 2c shows the resulting force/displacement curve obtained from this procedure. As expected, the curve is antisymmetric about the y axis. While the harvester displacement is approximately linear near the equilibrium point, the response "stiffens" as the magnet moves further away from equilibrium. To mathematically define this interesting force/displacement relationship, both a cubic polynomial and a fifth-order polynomial were fit to this data. The resulting polynomials are:

$$F_1(x_o) = 110x_0 + 3.52e5x_0^3 \tag{1}$$

$$F_2(x_o) = 85x_0 - 2.36e5x_0^3 + 7.06e8x_o^5 \tag{2}$$

Where x_0 is the central magnet's displacement (in meters) from the midpoint between the top and bottom magnets and F is the resulting restoring force in Newtons. Both approximations will be used in developing a mathematical model for the system.

2.3 Development of Linear Energy Harvester

In order to make a comparison with the nonlinear energy harvester, a linear energy harvester is also constructed. To provide the best comparison, this linear energy harvester should have a natural frequency close to the natural frequency of the linear harvester. The damping ratio ζ of both systems should be made as close as possible as well. Section 4.2 details the fabrication of the linear device.

3. MATHEMATICAL MODEL OF ELECTROMAGNETIC ENERGY HARVESTER

In order to predict the performance of both the nonlinear and linear energy harvesting systems, the governing equations of motion are derived.

Consider the free body and circuit diagrams for the nonlinear harvester, shown in Fig. 3. The absolute displacement from the static equilibrium position is $x(t)$, while the displacement of the base under excitation is $y(t)$. The mass of the center magnet, including the rod emanating out of the harvester, is defined as m. The restoring force due to the magnet configuration can be modeled as a spring with a linear component k_1 and nonlinear components k_3 and k_5. The system's mechanical damping can be modeled as linearly proportional to the relative velocity $\dot{x}(t) - \dot{y}(t)$, with a mechanical damping constant c_m. This term accounts for all mechanical energy losses in the system. As the permanent magnet oscillates past the coil of wire wrapped around the harvester, a current i is generated within the coil, resulting in energy being removed from the system in the form of electricity. This energy removal is modeled by using the equation for the mechanical force generated by a coil of wire moving through a magnetic field:

$$F_m = Ki \tag{3}$$

Where $K = NBl$, N is the number of coil turns, B is the magnetic field in the air gap between the mass and the coil, which is assumed uniform and constant in time,[12] and l is the length of wire per turn.

Applying Newton's law to the central magnet, the governing equation of motion can be expressed as:

$$m\ddot{x} + c_m(\dot{x} - \dot{y}) + k_1(x - y) + k_3(x - y)^3 + k_5(x - y)^5 + Ki = -mg \tag{4}$$

The current generated within the coil of wire flows through the equivalent circuit for the harvester, also shown in Fig. 3. The coil is modeled as having a resistance R_{coil} and inductance L. The electrical power generated from the harvester is dissipated across a load resistor R_{load}. Applying Kirchoff's Voltage law to the circuit yields the following equation:

$$(R_{coil} + R_{load})i = K(\dot{x} - \dot{y}) \tag{5}$$

Note that we have neglected to account for the coil inductance, as the harvesting coil we used experimentally had an inductance on the order of a few mH, which is small enough to be neglected.[13] Additionally, note the $K(\dot{x} - \dot{y})$ term in Eq. 5. This term refers to the "back-emf" e_b generated by the motion of the central magnet past the coil of wire, given by Faraday's Law:

$$e_b = -\frac{d(\Phi B)}{dt} = NBl(\dot{x} - \dot{y}) = K(\dot{x} - \dot{y}) \tag{6}$$

Note that Eq. 5 can be solved for i and combined with Eq. 4, resulting in the following governing equation:

$$m\ddot{x} + c_{tot}(\dot{x} - \dot{y}) + k_1(x - y) + k_3(x - y)^3 + k_5(x - y)^5 = -mg \tag{7}$$

Where the transfer of energy from the mechanical to electrical domain is now modeled as a damping term within the total system damping $c_{tot} = c_m + c_e$, where c_e is given by:

$$c_e = \frac{K^2}{R_{coil} + R_{load}} \tag{8}$$

The amount of energy that is extracted from the environment and delivered as useful power is given by:

$$P(t) = i^2 R_{load} = \frac{c_e}{K}(\dot{x} - \dot{y}) \tag{9}$$

We now have a pair of nonlinear, second order differential equations we can use to solve for the displacement and velocity of the center magnet as well as the resulting generated power. Note that for the linear harvester, the nonlinear terms in Eq. 7 go to 0 and the displacement and velocity of the central mass can be obtained with the familiar second order differential equation for the forced response of a mass/spring/damper system:

$$\ddot{x} + 2\zeta\omega_n(\dot{x} - \dot{y}) + \omega_n^2(x - y) = -g \tag{10}$$

Where ω_n is the natural frequency and ζ the total system damping ratio. We will directly integrate Eq. 7 to obtain x and $\dot{x}$ and use the results to compute $P(t)$. Note that for the case where the cubic polynomial for the restoring force is used, Eq. 7 simplifies to Duffing's equation for nonlinear oscillators. Several techniques are available to obtain accurate approximations of closed-form solutions to Duffing's Equation (see Refs. 9 and 14), but these will not be investigated here.

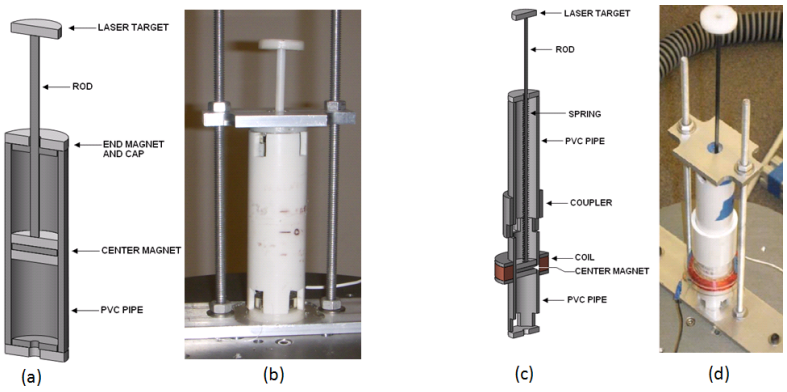

Figure 4. (a) CAD model showing the nonlinear energy harvester design. (b) Picture of fabricated nonlinear harvester. (c) CAD model of linear energy harvester. Slots cut into the pipe above and below the coil vent air during operation to eliminate viscous damping effects. (d) Picture of linear energy harvester.

4. EXPERIMENTAL INVESTIGATION

4.1 Fabrication of Nonlinear Harvester

A CAD drawing and photograph of the nonlinear electromagnetic harvester fabricated for experimental testing is shown in Fig. 4(a) and (b). The device was constructed with PVC piping and three circular neodymium magnets. The neodymium magnets have a hollowed-out center, enabling a laser target fixed to the oscillating magnet to protrude from the device so that measurements can be taken with an optical displacement sensor.

The coil used to generate electrical current was fabricated by using a coil-winding apparatus to wrap 26 AWG wire between two acrylic discs located outside the PVC tubing, centered at the equilibrium position of the magnet. The two ends of the coil were connected via a 4.4Ω load resistor that matched the resistance of the coil. It can be shown that power dissipated by a harvester is maximized when the load resistance R_{load} matches the coil resistance R_{coil}.[1]

4.2 Fabrication of Linear Harvester

A CAD drawing and photograph of the linear harvester is shown in Fig. 4(c) and (d).

To make the linear and nonlinear devices comparable in terms of natural frequency and damping ratio, the same type of magnet and fabrication components were used to ensure the linear system would function as similarly as possible to the nonlinear one. To achieve the desired natural frequency, a continuous spring was cut to the length that gave the desired spring constant. An additional PVC pipe was also cut to length such that the linear harvester had the same equilibrium position as the nonlinear harvester. The device shown in Fig. 4(d) has a natural frequency of 8.55 Hz.

4.3 Experimental Test Setup

The energy harvesters were secured to a Labworks ET-140 shaker table using entirely aluminum components to avoid interference with the nonlinear harvester's strong magnets. A MicroEpsilon LD1607-200 optical displacement sensor was used to measure the dynamic response of the harvester when driven with a shaker input, while an oscilloscope was used to compute the RMS voltage across the load resistor, enabling measurements of average dissipated power. An aluminum structure was used to hold the displacement sensor directly over the harvester, sensing the displacement of the laser targets attached to the oscillating magnet for both harvesters.

4.4 Comparison of Simulated and Experimental Frequency Response

Frequency response data was experimentally taken for both the nonlinear and linear harvesters by performing a frequency sweep with the shaker table. The input displacement $y(t)$ was set to be a sinusoid with constant amplitude of .0.51 cm (2") peak to peak, while the range of driving frequencies was varied from 5-11 Hz, with enough dwell time at each frequency to ensure a steady state response. The resulting peak-to-peak displacement was measured at each dwell frequency as well as the peak-to-peak voltage and the RMS power dissipated across R_{load}. The experimentally obtained frequency responses for the linear harvester is compared to the results from numerical integration of the governing equations in Figs. 5 and 6. Table 1 shows the parameter values measured for both linear and nonlinear systems.

The experimental results for the linear harvester behave as expected for a linear second-order system with low damping ratio. The peak-to-peak displacement reaches a maximum of around 8 cm at the device resonant frequency (8.55 Hz), with maximum values of peak-to-peak voltage (.9 V) and RMS power (15 mW) also occurring at this frequency. As is characteristic of such systems, very little power is generated off resonance, with a half-power bandwidth of only 0.4 Hz.

Table 1. Experimental parameter values measured for linear and nonlinear energy harvesters. Damping ratio was obtained for linear harvester via half-power method and for nonlinear harvester via logarithmic decrement. Note that determination of mass and spring constant for linear harvester is not necessary.

Parameter	**Linear Harvester**	**Nonlin. Harvester**	**Units**
m	N/A	.0256	kg
k_1	N/A	85	N/m
k_3	N/A	-2.365e3	N/m^3
k_5	N/A	7.066e8	N/m^5
ω_n	53.41	57.622	rad/s
ζ	.0197	.0308	–
c_{tot}	.0614	.0793	N s/m
c_e	.0334	.0281	N s/m
K	.5419	.4968	V s/m
R_{load}	4.4	4.4	Ω
R_{coil}	4.4	4.4	Ω

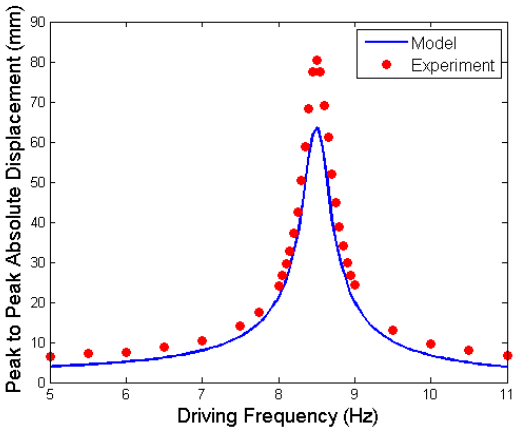

Figure 5. Experimentally determined frequency response for $x(t)$ is compared with predicted results from direct numerical integration.

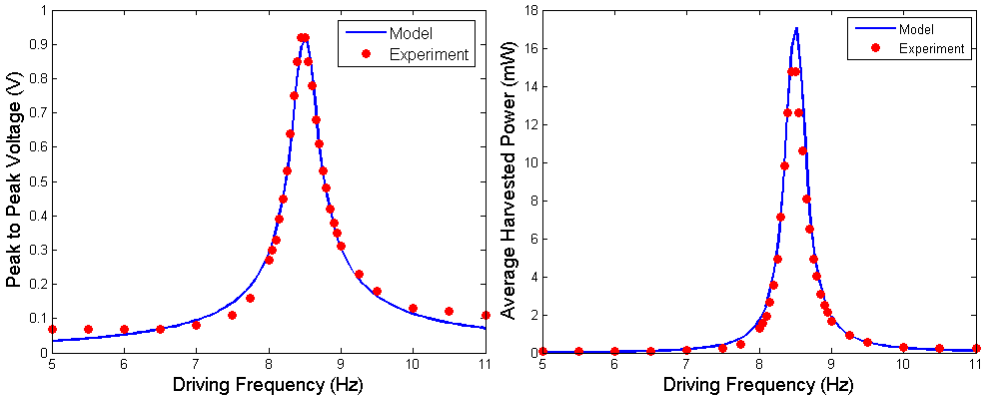

Figure 6. (Left) Experimentally determined frequency response of peak-to-peak voltage across R_{load} is compared with predicted results from direct numerical integration. (Right) Harvested power as a function of input driving frequency for both experiment and simulation.

The predicted results obtained from direct numerical integration generally agree well with the experimental results, with two noteworthy anomalies. First, the peak-to-peak displacement predicted by both numerical simulation and analytical solutions of Eq. 10 is 65 mm at resonance, which does not match the observed resonant peak-to-peak displacement of 80 mm at resonance. This is interesting because the observed resonant voltage across R_{load} matches very well with the predicted value from numerical integration. This anomaly is most likely explained by the long sample time (40 s) used to find the peak-to-peak displacement - it is possible the oscilloscope reading the displacement sensor picked up on an outlying displacement value.

Figs. 7 and 8 show the corresponding frequency responses for the nonlinear harvester. Note that for the simulation, the fifth order polynomial in Eq. 2 was used over its third order counterpart as it shows better agreement with the force/displacement data in Fig. 2. A cursory glance at the results indicates that there are significant differences in the frequency response of the harvester due to the addition of nonlinear terms in the governing equations of motion. Fig. 7 shows that the frequency response has the form of a "backbone curve" typical of Duffing oscillators.[14] The "hardening" or bending of the curve to the right is caused by the nonlinear stiffness.

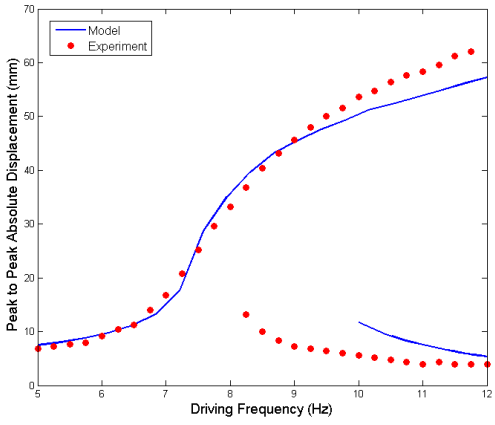

Figure 7. Peak-to-peak displacement is shown over a range of driving frequencies for both the nonlinear harvester experiment and numerical simulation. Note the characteristic "backbone" shape seen for the frequency response of nonlinear oscillators.

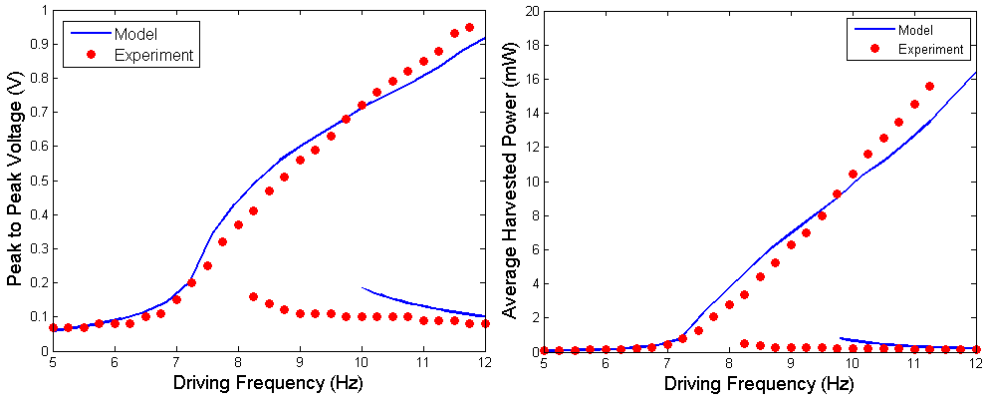

Figure 8. (Left) Experimentally determined peak-to-peak voltage across R_{load} compared with simulation results for nonlinear harvester. (Right) Harvested power for both experiment and simulation.

There is a hysteretic region (approximately 8 Hz -12 Hz) where two stable, steady-state, periodic responses co-exist. Perturbations to the system can cause a switch between response branches. In this hysteretic region, the response of the system exhibits jump phenomena where the amplitude of oscillation jumps between response branches as the excitation frequency is increased or decreased. The agreement between the experiment and numerical integration is generally good for all three frequency responses, but one interesting discrepancy of note is that the "jump frequency" where multiple stable solutions appear is higher for the simulation when compared to the experimental data.

5. COMPARING NONLINEAR AND LINEAR DEVICE

As Fig. 8 indicates, the characteristic backbone shape of a Duffing oscillator corresponds to increased power harvesting bandwidth. Figure 9 shows the power generation of the linear harvester compared with that of the nonlinear harvester. Both harvesters have similar peak power generation, but the nonlinear harvester clearly has significantly higher bandwidth. Based on Fig. 9 alone, it would seem like an obvious choice to prefer the nonlinear oscillator over the linear oscillator for most harvesting applications. However, several drawbacks exist to the nonlinear harvester configuration that were not fully investigated in other studies (See Refs. 8 and 9). The most significant of these is that the nonlinear oscillator has more than one stable solution after the jump frequency.

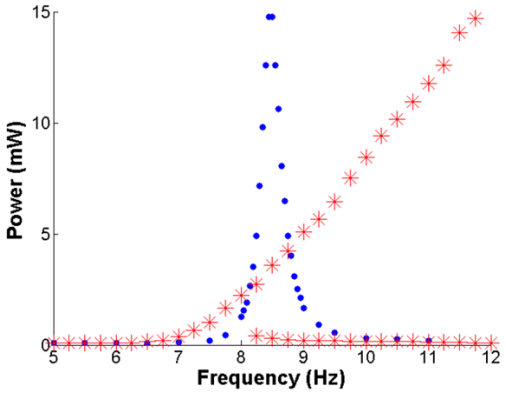

Figure 9. Power generation of nonlinear harvester (red asterisks) compared to linear harvester (blue dots). Note that results are from harmonic frequency sweeps.

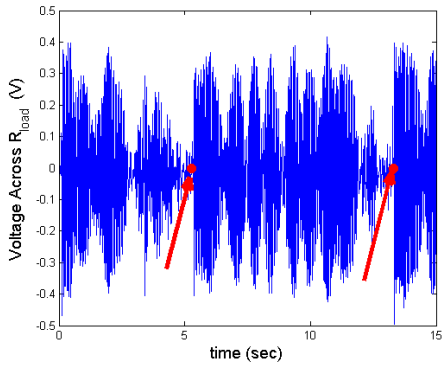

Figure 10. Time response of nonlinear harvester voltage generation when subjected to uniform random vibration input with frequency range 9-11 Hz and input amplitude .2 g^2/Hz. Arrows indicate where a perturbation was required to maintain high amplitude oscillation.

While it would be desirable for the harvester to operate only along the high displacement/power curve, the nonlinear harvester in reality tends toward the low amplitude steady state solution as it is a lower energy state. Mann et. al reports that the high amplitude curve can be selected through a perturbation or energy excitement of the harvester. Our experiments confirmed this, as we were able to remain indefinitely at high amplitude solutions by initially giving a tap to the protruding laser target by hand. However, it should be kept in mind that this is for *harmonic* excitation only. As mentioned earlier, most real vibration profiles are random and occur across a spectrum of frequencies. Therefore, we might expect that the time-varying nature of real frequency spectra might knock the oscillator back to the low energy state, requiring multiple sustained perturbations to maintain high power harvesting levels. This hypothesis is further evaluated in the next section.

5.1 Response to Random Excitation

To test our hypothesis that random excitation might keep the nonlinear harvester from continuously operating in the higher energy state, we subjected the harvester to various "white noise" vibration spectra. Figure 10 shows a characteristic time response obtained from such a random vibration input. The time response shows that the nonlinear harvester is still able to reach high displacement values when an initial perturbation is provided. However, after a certain length of time, the response then drops back to the lower energy state, and an impulse of energy must again be provided. This was not observed when the input vibration was harmonic, in which case the nonlinear harvester was able to oscillate indefinitely at the high energy state once given an initial perturbation. We noticed that for very narrow input frequency bandwidths (i.e. $<$ .3 Hz), the average time for which the oscillator remained in the high energy state was around 20 seconds after a perturbation was provided. However, as the input vibration was spread over a wider frequency bandwidth, we noticed a very rapid increase in the number of perturbations needed per unit time to sustain the high energy state.

With this limitation of the nonlinear harvester in mind, the performance of the nonlinear harvester was compared to that of the linear harvester by performing a series of random vibration tests with varying input frequency ranges. For these tests, we assumed the nonlinear harvester could be given an impulse as often as necessary to maintain high amplitude oscillations. Looking at Fig. 9, we would expect the linear harvester to significantly outperform the nonlinear harvester when the random vibration spectrum was centered around the linear harvester's resonant frequency. However, for input frequency ranges that extended past the resonant frequency, we would expect to see the nonlinear harvester outperforming the linear harvester. Random vibration tests were therefore performed over a large number of frequency ranges and bandwidths, with the average power generated from both harvesters computed after a sample time of 40 seconds. The number of impulses required to maintain the nonlinear oscillator in a high amplitude state for each test was also recorded. Results of these tests are shown in Table 2.

Several conclusions can be drawn from Table 2. The first three tests have uniform input vibration in the 6-12 Hz range, spanning the entire frequency range shown in Fig. 9. For these tests, the linear harvester outperforms

Table 2. Measured power for linear and nonlinear harvesters. "Number of Impulses" gives approximate number of perturbations required to maintain high amplitude oscillation in nonlinear oscillator. Where number is not listed, such oscillations could not be maintained so no impulses were given.

Test	**Freq. (Hz)**	**Acceleration (g^2/Hz)**	**Nonlinear Power (mW)**	**# Impulses**	**Linear Power (mW)**
1	6 to 12	.02	1.63	0	**2.45**
2	6 to 12	.04	2.31	0	**3.60**
3	6 to 12	.08	3.96	0	**4.10**
4	8 to 11	.08	3.55	4	**4.97**
5	6 to 9	.04	1.84	2	**3.38**
6	7 to 10	.04	2.70	0	**3.43**
7	8 to 9	.15	3.66	0	**7.61**
8	9 to 11	.2	**4.58**	4	1.85
9	9 to 11.5	.2	**2.5**	8	1.34
10	9.5 to 11.5	.2	**2.27**	8	.68
11	10 to 10.2	2	**6.47**	1	.705

the nonlinear harvester, although the power generated by the nonlinear harvester approaches the linear harvester as the input vibration amplitude is increased. This is because higher amplitude input oscillations are more likely to excite the high energy response of the nonlinear harvester. For this 6 Hz frequency bandwidth, providing impulses to the nonlinear harvester had no noticeable effect.

In tests 4-7, the frequency bandwidth is narrowed to a range encompassing the resonant peak of the linear harvester and a portion of the high amplitude region of the nonlinear harvester. The results show that the linear harvester still generates more power than the nonlinear harvester. For the case where the input frequency range is 8-9 Hz, encompassing only the resonant peak of the linear harvester, the result is a nearly 2 to 1 ratio of generated power between the two harvesters.

The last four tests show the results of shifting the input frequency range well above the resonant frequency of the linear harvester, into the nonlinear harvester's high-amplitude region. As expected, under these conditions the nonlinear harvester generates significantly more power than the linear harvester. However, the nonlinear harvester requires continuous energy impulses to maintain high amplitude oscillations because the bandwidth of input vibration is several Hz. However, for the final test, where the input vibrations range from 10-10.2 Hz, the bandwidth is small enough to be approximated as harmonic, and the nonlinear harvester can generate significant power without needing a high number of impulses.

6. CONCLUSION: APPLICATIONS FOR NONLINEAR ENERGY HARVESTERS

The results from the modeling and experimental testing of the three-magnet energy harvester can be used to consider the benefits and drawbacks of using a nonlinear oscillator as an energy harvesting device. While there are a variety of nonlinear oscillator types, many are characterized well by a high order polynomic force/displacement relationship and tend to display the characteristic "backbone" frequency response predicted by Duffing's Equation.

While such nonlinear oscillators have been proposed as a mechanism to effectively harvest energy over a wide bandwidth of input frequencies, our studies have shown that the existence of multiple stable solutions creates an undesirable tendency for the nonlinear harvester to prefer the lowest energy state. While we found that an initial perturbation can move the nonlinear harvester to the higher energy state, the nonlinear harvester can only maintain this state if the input vibration can be approximated as a sinusoid. For random broadband inputs, abrupt changes in the vibration time response causes the harvester to revert back to the low energy state after several seconds, requiring the external input of continuous energy impulses to maintain high amplitude oscillations.

Therefore, the nonlinear harvester may actually have a better use in situations where the ambient vibration is dominated by a single frequency whose exact location is unknown or changes with time. In these situations, using a single-degree-of-freedom linear harvester at the predicted resonant frequency amounts to nothing more than an educated guess. If the actual vibration frequency is different than the predicted frequency by even a small amount, or changes slightly over time, the linear harvester will see a significant drop in harvested power. However, designing a nonlinear harvester such that the expected vibration frequency occurs in the middle of the harvester's broadband frequency response curve provides a good margin of error. If the dominant vibration frequency shifts slightly or is different from what was expected, the nonlinear harvester will still be capable of providing a high level of output power.

However, it should be noted that many ambient vibration environments are *not* well characterized by a simple harmonic excitation. In such cases, broadband harvesting is still a necessity. For the three-magnet nonlinear harvester developed here, broadband harvesting capability is limited by the fact that constant perturbations are required to keep the nonlinear harvester from reverting to low amplitude oscillations. Automating these input perturbations would require an active control system, with both a mechanism of measuring when the system is at a low amplitude state and an actuation mechanism to provide the needed energy impulse. Increasing the feasibility of such a nonlinear harvester therefore requires further work to either decrease the number of required perturbations or to develop an actuation system that can provide the necessary perturbations at a low energy cost.

REFERENCES

[1] Roundy, S., Wright, P., and Rabaey, J., [*Energy Scavenging for Wireless Sensor Networks: with Special Focus on Vibrations*], Springer, Norwell, Mass. (2003).

[2] Xu, N., "A survey of sensor network applications," *IEEE Communications Magazine* **40** (2002).

[3] duToit, N. and Wardle, B., "Experimental verification of a coupled electromechanical model for mems piezoelectric vibration energy harvesters," in [*Structures, Structural Dynamics, and Materials*], *AIAA Journal* **45** (2007).

[4] Ferro Solutions, I., "Veh 360 data sheet." Online at http://www.ferrosi.com/.

[5] Roundy, S., Leland, E. S., Baker, J., Carleton, E., Reilly, E., Lai, E., Otis, B., Rabaey, J. M., Sundararajan, V., and Wright, P. K., "Improving power output for vibration-based energy scavengers," *IEEE Pervasive Computing* **4**, 28–36 (2005).

[6] Alper Erturk, J. M. R. and Inman, D. J., "Modeling of piezoelectric energy harvesting from an l-shaped beam-mass structure with an application to uavs," *Journal of Intelligent Material Systems and Structures* **20**(5) (2008).

[7] Alper Erturk, J. M. R. and Inman, D. J., "Piezoelectric energy harvesting from an l-shaped beam-mass structure," in [*Active and Passsive Smart Structures and Integrated Systems*], Ahmadian, M., ed., Proc. SPIE (2008).

[8] Erturk, A., Hoffman, J., and Inman, D., "A piezomagnetoelastic structure for broadband vibration energy harvesting," *Applied Physics Letters* **94** (June 2009).

[9] B.P. Mann, N. S., "Energy harvesting from the nonlinear oscillations of magnetic levitation," *Journal of Sound and Vibration* **319**, 515–530 (2009).

[10] Defrancesco, S. and Zanetti, V., "Experiments on magnetic repulsion," *Am. J. Phys.* **51**(11), 1023–1025 (1983).

[11] Domme, D. J., *Experimental and Analytical Characterization of a Transducer for Energy Harvesting Through Electromagnetic Induction*, Master's thesis, Virginia Polytechnic Institute and State University (April 2008).

[12] Beeby, S., Tudor, M., Torah, R., Koukharenko, E., Roberts, S., O'Donnell, T., and Roy, S., "Macro and micro scale electromagnetic kinetic energy harvesting generators," in [*Symposium on Design, Test, Integration and Packaging of MEMS/MOEMS*], IEEE (2006).

[13] Stephen, N., "On energy harvesting from ambient vibration," *Journal of Sound and Vibration* **293**, 409–425 (December 2006).

[14] Rao, S. S., [*Mechanical Vibrations*], Prentice Hall, Upper Saddle River, New Jersey (1995).